Earthquakes and Structures, *Vol. 7, No. 5 (2014) 627-645*
DOI: http://dx.doi.org/10.12989/eas.2014.7.5.627

Constitutive models of concrete structures subjected to seismic shear

Arghadeep Laskar[1], Liang Lu[2], Feng Qin[3], Y.L. Mo[*4], Thomas T.C. Hsu[4], Xilin Lu[2] and Feng Fan[3]

[1]*Department of Civil Engineering, Indian Institute of Technology Bombay, Powai, Mumbai 200076, India*
[2]*Institute of Structural Engineering and Disaster Reduction, Tongji University, Shanghai, 200092, China*
[3]*School of Civil Engineering, Harbin Institute of Technology, Harbin, 150090, China*
[4]*Department of Civil and Environmental Engineering, University of Houston, Houston, 77204-4003, USA*

(Received December 17, 2014, Revised December 5, 2014, Accepted February 26, 2014)

Abstract. Using OpenSees as a framework, constitutive models of reinforced, prestressed and prestressed steel fiber concrete found by the panel tests have been implemented into a finite element program called Simulation of Concrete Structures (SCS) to predict the seismic behavior of shear-critical reinforced and prestressed concrete structures. The developed finite element program was validated by tests on prestressed steel fiber concrete beams under monotonic loading, post tensioned precast concrete column under reversed cyclic loading, framed shear walls under reversed cyclic loading or shaking table excitations, and a seven-story wall building under shake table excitations. The comparison of analytical results with test outcomes indicates good agreement.

Keywords: constitutive models; reinforced and prestressed concrete structures; finite element analysis

1. Introduction

Shear is one of the most critical aspects in seismic design of concrete structures. Lu *et al*. (2012) and Xing *et al*. (2013) studied shear in reinforced concrete beam-column joints through experiments and found that shear reinforcement can reduce cracks in beam-column joints. Moretti and Tassios (2013) critically examine the code provisions for shear design of short columns. The past three decades have seen a rapid development of knowledge in shear of reinforced concrete (RC) structures. Various rational models have been proposed that are based on the smeared-crack concept and can satisfy Navier's three principles of mechanics of materials (i.e., stress equilibrium, strain compatibility and constitutive laws). These rational or mechanics-based models on the "smeared-crack level" (in contrast to the "discrete-crack level" or "local level") include the compression field theory (CFT) (Vecchio and Collins 1981), the modified compression field theory (MCFT) (Vecchio and Collins 1986), the rotating-angle softened truss model, (RA-STM) (Hsu 1993, Belarbi and Hsu 1995, Pang and Hsu 1995), the fixed-angle softened truss model, (FA-STM) (Hsu and Zhang 1996, Pang and Hsu 1996), the softened membrane model, (SMM) (Zhu *et*

*Corresponding author, Professor, E-mail: E-mail:ymo@uh.edu.

 ISSN: 2092-7614 (Print), 2092-7622 (Online)

al. 2001, Zhu and Hsu 2002), and the cyclic softened membrane model, (CSMM) (Mansour 2001, Hsu and Mansour 2005, Mansour and Hsu 2005a, 2005b).

Vecchio and Collins (1981) proposed the earliest rational theory CFT, to predict the nonlinear behavior of cracked RC membrane elements. However, the CFT was unable to take into account the tension stiffening of the concrete in the prediction of deformations because the tensile stress of concrete was assumed to be zero. In 1986 the MCFT was proposed to include a relationship for concrete in tension to better model the stiffness of experiments.

The RA-STM, a rational theory developed at the University of Houston (UH) in 1995, had two improvements over the CFT: (1) The tensile stress of concrete was taken into account so that the deformations could be correctly predicted, and (2) the smeared (or average) stress-strain curve of steel bars embedded in concrete was derived on the "smeared crack level" so that it could be correctly used in the equilibrium and compatibility equations which are based on continuous materials.

By 1996 the UH group reported the FA-STM that is capable of predicting the "concrete contribution" (Vc) by assuming the cracks to be oriented at the fixed angle. Zhu *et al*. (2001) derived a rational shear modulus and produced a solution algorithm of FA-STM that is as simple as that of RA-STM.

Another significant advancement has come with the improvements on the softened truss models (rotating-angle and fixed-angle). As they were, these models could predict the ascending response curves of shear panels, but not the post-peak descending curves. By incorporating the Poisson effect of cracked RC (characterized by two new Hsu/Zhu ratios), the Softened Membrane Model (SMM) was developed which can satisfactorily predict the entire monotonic response curves, including both the ascending and descending branches (Hsu and Zhu 2002).

Fifteen RC elements (panels) under reversed cyclic shear stresses, were tested by (Mansour and Hsu (2005a), 2005b). Based on these test results, the Cyclic Softened Membrane Model (CSMM) was proposed to rationally predict the hysteretic loops of RC. The CSMM can accurately predict the pinching effect, the shear ductility and the energy dissipation capacities of the two-dimensional membrane element (Hsu and Mansour 2005). For these reasons, CSMM is the most appropriate model to be implemented into the OpenSees platform (OpenSees 2013) for the prediction of the cyclic shear force-displacement behavior of walls (or other two-dimensional structures) where shear deformations are significant. In recent years the SMM has also been extended to prestressed concrete (PC) and prestressed steel fiber concrete (PSFC) to develop SMM-PC (Wang 2006, Hoffman 2010). This can be used in conjunction with the CSMM to rationally predict the hysteresis loops for two-dimensional shear critical prestressed concrete structures. Research efforts to extend the application of these two-dimensional models to three-dimensional structures are currently under execution.

In this paper, the introduction of CSMM for RC, PC and PSFC is presented, including the equilibrium and compatibility equations, the constitutive relationships of the materials and finite element implementation. Five sets of constitutive relationships are summarized, namely reinforced concrete, prestressed concrete, embedded mild steel bars, embedded prestressing tendons and prestressed steel fiber concrete. In the finite element implementation section, the element formulation is derived. Adopting the OpenSees as the finite element framework, a finite element program named SCS (Simulation of Concrete Structures) (Mo *et al*. 2008) developed for RC was extended to include PC and PSFC. Lastly the SCS was validated through comparison between the test results and simulated outcomes.

(a) Applied principal stresses in local coordinate

(b) Reinforcement component in local coordinate

Fig. 1 Coordinate systems for RC and PC element

2. Cyclic softened membrane model (CSMM) for RC, PC and PSFC

The cyclic softened membrane model was first developed by Mansour and Hsu (2005b) for reinforced concrete structures. This paper extends the CSMM to include prestressed concrete and prestressed steel fiber concrete structures.

2.1 Coordinate system in CSMM

Three Cartesian – coordinates, *x–y*, 1–2, and $x_{si} - y_{si}$, are defined in the reinforced/prestressed concrete elements, as demonstrated in Fig. 1 (Hsu and Mo 2010).Coordinate *x–y* represents the local coordinate of the elements. The coordinate 1–2 defines the principal stress directions of the applied stresses, which have an angle θ_1 with respect to the $x - y$ coordinate. Steel bars can be distributed in different directions in the concrete. Coordinate $x_{si} - y_{si}$ shows the 'ith' direction of the reinforcing steel bars, where the 'ith' steel bars are located in the direction of axis x_{si} at an angle θ_{si} to the $x - y$ coordinate. Stresses and strains can be transformed between coordinate systems using transformation matrix $[T(\alpha)]$ given in Eq. 1.

$$[T(\alpha)] = \begin{bmatrix} c^2 & s^2 & 2sc \\ s^2 & c^2 & -2sc \\ -sc & sc & c^2 - s^2 \end{bmatrix} \tag{1}$$

where α is the angle from the original coordinate to the new coordinate, $c = \cos(\alpha)$ and $s = \sin(\alpha)$.

2.2 Equilibrium equations

The equilibrium equation that relates the applied stresses in the x–y coordinate (σ_x, σ_y and τ_{xy}) to the internal concrete stresses σ_1^c, σ_2^c and τ_{12}^c) in the principal stress directions, and the steel bar stresses (f_{si}) in the bar directions is expressed in Eq. (1).

$$\begin{bmatrix} \sigma_x \\ \sigma_y \\ \tau_{xy} \end{bmatrix} = [T(-\theta_1)] \begin{bmatrix} \sigma_1^c \\ \sigma_2^c \\ \tau_{12}^c \end{bmatrix} + \sum_i [T(-\theta_{si})] \begin{bmatrix} \rho_{si} f_{si} \\ 0 \\ 0 \end{bmatrix} \tag{2}$$

where ρ_{si} is the steel ratio in the 'ith' direction, $[T(-\theta_1)]$ and $[T(-\theta_{si})]$ are the transformation matrices from the 1–2 coordinate and the $x_{si} - y_{si}$ coordinate to the $x - y$ coordinate, respectively.

2.3 Compatibility equations

The compatibility equation, which represents the relationship between the steel strains (ε_{si}) in the $x_{si} - y_{si}$ coordinate and the concrete strains (ε_1, ε_2, and $\gamma_{12}/2$) in the 1–2 coordinate, is given in Eq. (3) ε_1, ε_2 and ε_{si} are biaxial strains, taking into account the Hsu/Zhu ratios of cracked reinforced concrete (Zhu and Hsu 2002).

$$\begin{bmatrix} \varepsilon_{si} \\ \varepsilon_{si'} \\ \frac{\gamma_{si}}{2} \end{bmatrix} = [T(\theta_{si} - \theta_1)] \begin{bmatrix} \varepsilon_1 \\ \varepsilon_2 \\ \frac{\gamma_{12}}{2} \end{bmatrix} \tag{3}$$

where $[T(\theta_{si} - \theta_1)]$ is the transformation matrix from the $1-2$ coordinate to the $x_{si} - y_{si}$ coordinate, and $\varepsilon_{si'}$ and γ_{si} are the smeared Poisson effect and the smeared dowel action for the steel bars in the 'ith' direction, which are neglected in the CSMM.

2.4 Biaxial srains vs. Uniaxial strains

To solve the equilibrium Eq. 2 and compatibility Eq. 3, the stress-strain relationships of concrete and steel have to be based on the biaxial strains ε_1, ε_2 and ε_{si}. Since general laboratory experiments can provide only the uniaxial constitutive relationships of concrete and steel (rather than the biaxial constitutive relationships), the biaxial strains in Eq. 3 must be converted to uniaxial strains before the uniaxial constitutive relationships can be utilized. Thus, Eqs.4 to 6 have been derived by Zhu and Hsu (2002) to relate the set of biaxial strains (ε_1, ε_2, and ε_{si}) to the set of uniaxial strains ($\bar{\varepsilon}_1$, $\bar{\varepsilon}_2$ and $\bar{\varepsilon}_{si}$) using the Hsu/Zhu ratios (ν_{12}, ν_{21}).

$$\begin{bmatrix} \bar{\varepsilon}_1 \\ \bar{\varepsilon}_2 \\ \frac{1}{2}\gamma_{12} \end{bmatrix} = [V] \begin{bmatrix} \varepsilon_1 \\ \varepsilon_2 \\ \frac{1}{2}\gamma_{12} \end{bmatrix} \tag{4}$$

$$[V] = \begin{bmatrix} \frac{1}{1-\nu_{12}\nu_{21}} & \frac{\nu_{12}}{1-\nu_{12}\nu_{21}} & 0 \\ \frac{\nu_{21}}{1-\nu_{12}\nu_{21}} & \frac{1}{1-\nu_{12}\nu_{21}} & 0 \\ 0 & 0 & 1 \end{bmatrix} \tag{5}$$

The uniaxial strain of steel ($\bar{\varepsilon}_{si}$) can be obtained by transforming uniaxial strains of concrete ($\bar{\varepsilon}_1$ and $\bar{\varepsilon}_2$) using Eq .6.

$$\begin{bmatrix} \bar{\varepsilon}_{si} \\ \bar{\varepsilon}_{si'} \\ \frac{\gamma_{si}}{2} \end{bmatrix} = [T(\theta_{si} - \theta_1)] \begin{bmatrix} \bar{\varepsilon}_1 \\ \bar{\varepsilon}_2 \\ \frac{\gamma_{12}}{2} \end{bmatrix} \tag{6}$$

Once the uniaxial strains $\bar{\varepsilon}_1$, $\bar{\varepsilon}_2$ and $\bar{\varepsilon}_{si}$ are determined, the stresses σ_1^c, σ_2^c, τ_{12}^c and f_{si} in Eq.

(2) can be calculated using the uniaxial constitutive relationships of materials.

2.5 Constitutive models

2.5.1 Uniaxial constitutive relationship of concrete in RC/PC

The cyclic uniaxial constitutive relationships of cracked concrete in compression and tension are summarized in Fig. 2. In the graph, the vertical axis represents the cyclic stress σ^c, with positive tensile stress above the origin and negative compressive stress below the origin. The horizontal axis represents the cyclic uniaxial strain $\bar{\varepsilon}$, with positive tensile strain to the right of origin and negative compressive strain to the left of origin.

The upper right quadrant gives the tensile envelope stress–strain curves T1 and T2. In the lower left quadrant is the compression envelope stress–strain curves C1 and C2. The unloading and reloading curves are represented by the series of straight lines C3-C7 in the compressive strain regions, and T3, T4 in the tensile strain region. Each straight line connects two points with their coordinates specified in the lower right quadrant.

Tension

In decompression (Stage UC) of PC, constitutive relationship are shown in Eq. (7) The tensile envelope curves, T1 and T2 in the biaxial condition, were found to be close to the monotonic curves. Since the tensile stress is very small compared with the compressive stress, the tensile envelope curves T1 and T2 are taken, for simplicity, to be the same as the monotonic curves expressed by Eqs (8) and (9).

$$\text{Stage UC} \quad \sigma^c = E_c'\bar{\varepsilon} + \sigma_{ci} \qquad \text{for PC only } \bar{\varepsilon} \le \bar{\varepsilon}_{cx} - \bar{\varepsilon}_{ci} \tag{7}$$

$$\text{Stage T1} \quad \sigma^c = E_c\left(\bar{\varepsilon} + \bar{\varepsilon}_{ci} - \bar{\varepsilon}_{cx}\right) \qquad \bar{\varepsilon}_{cx} - \bar{\varepsilon}_{ci} < \bar{\varepsilon} \le \varepsilon_{cr} - \bar{\varepsilon}_{ci} \tag{8}$$

$$\text{Stage T2} \quad \sigma^c = f_{cr}\left(\frac{\varepsilon_{cr}}{\bar{\varepsilon} + \bar{\varepsilon}_{ci}}\right)^{0.4} \qquad \bar{\varepsilon} > (\varepsilon_{cr} - \bar{\varepsilon}_{ci}) \tag{9}$$

where: E_c' is the decompression modulus of concrete, taken as kf_c'/ε_0, where k =1.4-1.5 and f_c' is maximum compressive stress of concrete obtained from standard cylinders,

σ_{ci} and $\bar{\varepsilon}_{ci}$ are initial compressive stress and strain in concrete due to prestress force, which are taken as zero for RC,

$\bar{\varepsilon}_{cx}$ is the extra strain in concrete after decompression, calculated by $\bar{\varepsilon}_{ci} - \sigma_{ci}/E_c'$,

ε_{cr} is the concrete cracking strain,

E_c is the modulus of concrete in tension before cracking,

f_{cr} is cracking stress of concrete, taken as $0.31\sqrt{f_c'(\text{MPa})}$.

Compression

The uniaxial compression constitutive relationships in stage C1 and C2 are shown in Eqs. (10) and (11) respectively.

$$\text{Stage C1} \quad \sigma^c = (D\zeta f_c' - f_{cT4}')\left[2\left(\frac{\bar{\varepsilon}}{\zeta\varepsilon_0}\right) - \left(\frac{\bar{\varepsilon}}{\zeta\varepsilon_0}\right)^2\right] + f_{cT4}' \qquad \zeta\varepsilon_0 \le \bar{\varepsilon} < 0 \tag{10}$$

$$\text{Stage C2} \quad \sigma^c = D\zeta f_c'\left[1 - \left(\frac{\bar{\varepsilon}/\varepsilon_0 - 1}{4/\zeta - 1}\right)^2\right] \qquad \bar{\varepsilon} < \zeta\varepsilon_0 \tag{11}$$

where: ζ is the softening coefficient, D is the damage coefficient,

ε_0 the concrete cylinder compressive strain at f_c',

f_{cT4}' is the concrete stress of point TD on the vertical axis at the end of stage T4.

When concrete stress did not reach stage T2, f_{cT4}' is zero, and the curve of stage C1 should go through the origin as shown in Fig. 2.

The softening coefficient can be determined by Eqs. (12) through (17)

$$\zeta = f_1(\bar{\varepsilon}_T)\, f_2(f_c')\, f_3(\beta) W_p W_f \tag{12}$$

where

$$f_1(\bar{\varepsilon}_T) = \frac{1}{\sqrt{1 + 400\bar{\varepsilon}_T}} \tag{13}$$

$$f_2(f_c') = \frac{5.8}{\sqrt{f_c'}} \le 0.9 \qquad \left(f' \text{ and } \sqrt{f_c'} \text{ in MPa}\right) \tag{14}$$

$$f_3(\beta) = 1 - \frac{|\beta|}{24^\circ} \tag{15}$$

$$W_p = \begin{cases} 1 & \text{for RC} \\ 1.15 + \dfrac{|\beta|(0.09|\beta| - 1)}{6} & \text{for PC and PSFC} \end{cases} \tag{16}$$

$$W_f = \begin{cases} 1 & \text{for RC and PC} \\ 1 + 0.2FF & \text{for PSFC} \end{cases} \tag{17}$$

where: $\bar{\varepsilon}_T$ is the uniaxial principal strain in tension,

β is the deviation angle, defined as $\beta = \alpha_r - \alpha_1$, where α_r is the angle from $\ell - t$ coordinate to $r - d$ coordinate which represents the direction of the principal stresses in concrete,

FF fiber factor in PSFC.

The damage coefficient is taken as a linear function of the compression strain ε'_c:

$$D = 1 - \psi\frac{\varepsilon'_c}{\varepsilon_0} \le 1.0 \tag{18}$$

where ε'_c (always negative) is the maximum compression strain normal to the compression direction under consideration, and occurred in the previous loading cycles. The symbol ψ is a constant taken as 0.4 to best fit the test results of the cyclic shear stress-strain curves of the test panels (Mansour 2001).

Unloading and reloading

The unloading and reloading curves, which can be applied to RC, PC and PSFC, are

constructed by connecting consecutively a set of points given in Fig. 2. The linear expression between two points is given as:

$$\sigma^c = \sigma_i^c + E_{cc}(\bar{\varepsilon} - \bar{\varepsilon}_i) \tag{19}$$

where σ_i^c and $\bar{\varepsilon}_i$ are concrete stress and strain at the load reverse point 'i' or at the point where the stages change; E_{cc} is the slope of linear expression and is taken to be

$$E_{cc} = \frac{\sigma_i^c - \sigma_{i+1}^c}{\bar{\varepsilon}_i - \bar{\varepsilon}_{i+1}} \tag{20}$$

where σ_{i+1}^c and $\bar{\varepsilon}_{i+1}$ are concrete stress and strain at the stage under consideration.

Shear

For a stress and strain analysis based on the smeared-crack concept, a rational and simple shear modulus as in Eq. (21) has been derived theoretically by Zhu *et al*. (2001), which can be applied to RC, PC and PSFC.

$$G_{12}^c = \frac{\tau_{12}^c}{\gamma_{12}/2} = \frac{\sigma_1^c - \sigma_2^c}{\varepsilon_1 - \varepsilon_2} \tag{21}$$

2.5.2 Uniaxial constitutive relationship of mild steel bar

The constitutive model for PSFC along with the factors that will affect PSFC are summarized in this section, including the constitutive relationships of cracked PSFC in tension and compression. The envelope curves are plotted in Fig. 4..These proposed constitutive relationships of PSFC takes into account the effect of presence of steel fibers in the concrete (Hoffman 2010).

Tension

The relationships of the stress σ^c versus the uniaxial strain $\bar{\varepsilon}$ of PSFC in tension are given in Eqs. 26 and 27.

Stage UC: $\sigma^c = E_c'\bar{\varepsilon}_1 + \sigma_{ci}$ $\bar{\varepsilon} \le (\bar{\varepsilon}_{cx} - \bar{\varepsilon}_{ci})$ (22)

Stage T1: $\sigma^c = E_c''(\bar{\varepsilon}_1 + \bar{\varepsilon}_{ci})$ $(\bar{\varepsilon}_{cx} - \bar{\varepsilon}_{ci}) < \bar{\varepsilon} \le (\varepsilon_{cy} - \bar{\varepsilon}_{ci})$ (23)

Stage T2: $\sigma^c = E_c'''(\bar{\varepsilon} + \bar{\varepsilon}_{ci})$ $(\bar{\varepsilon}_{cy} - \bar{\varepsilon}_{ci}) < \bar{\varepsilon} \le (\varepsilon_{cult} - \bar{\varepsilon}_{ci})$ (24)

Stage T3: $\sigma^c = E^{IV}{}_c(\bar{\varepsilon} + \bar{\varepsilon}_{ci})$ $\bar{\varepsilon} > (\varepsilon_{cult} - \bar{\varepsilon}_{ci})$ (25)

where: E_c' = decompression modulus of concrete taken as $2f_c'/\varepsilon_0$

$\bar{\varepsilon}_{ci}$ = initial strain in concrete due to prestress,

σ_{ci} = initial stress in PSFC,

$\bar{\varepsilon}_{cx}$ = extra strain in concrete after decompression calculated by $\bar{\varepsilon}_{ci} - \sigma_{ci}/E_c'$,

$\varepsilon_{c\max}$ = PSFC maximum strain taken as $0.04 - \varepsilon_{pi}$,

ε_{cult} = PSFC ultimate strain taken as $0.01 - \varepsilon_{pi}$,

ε_{pi} = strain at initial prestress,

f_{cult} = PSFC ultimate stress strain taken as $(0.2FF+12\rho_l)\sqrt{f_c'}$,

ε_{cy} = PSFC yield strain taken as 0.0005,

f_{cy} = PSFC effective "yield" stress for Proportional Loading, taken as $0.4*FF*CF\sqrt{f_c'}$, (f_c' and $\sqrt{f_c'}$ are in MPa), where CF = 1 for PSFC tensile volume confined (sandwiched) by two or more tendons, or CF = 0.5 for PSFC tensile volume unconfined by tendons,

E_c'' = modulus of PSFC taken as $f_{cy}/(\varepsilon_{cy}-\bar{\varepsilon}_{cx})$,

E_c''' = modulus of PSFC taken as $(f_{cult}-f_{cy})/(\varepsilon_{cult}-\varepsilon_{cy})$,

E_c^{IV} = modulus of PSFC taken as $-f_{cult}/(\varepsilon_{\max}-\varepsilon_{cult})$,

Compression

The smeared (average) constitutive relationships of PSFC stress σ^c and the uniaxial strain $\bar{\varepsilon}$ are given in Eqs. (26) and (27).

$$\sigma^c=\zeta f_c'\left[2\left(\frac{\bar{\varepsilon}}{\zeta\varepsilon_0}\right)-\left(\frac{\bar{\varepsilon}}{\zeta\varepsilon_0}\right)^2\right] \qquad \frac{\bar{\varepsilon}}{\zeta\varepsilon_0}\le 1 \tag{26}$$

or

$$\sigma^c=\zeta f_c'\left[1-\left(\frac{\bar{\varepsilon}/\zeta\varepsilon_0-1}{4/\zeta-1}\right)^2\right] \qquad \frac{\bar{\varepsilon}}{\zeta\varepsilon_0}>1 \tag{27}$$

where ζ is the softening coefficient, which can be determined in Eq. (12).

2.5.3 Uniaxial constitutive relationship of prestressing steel

The cyclic constitutive relationships of reinforcing steel bars embedded in concrete and subjected to uniaxial strains (Mansour *et al*. 2001) are summarized in Fig. 4. The solid curves represent the smeared stress–strain curves of steel bars, while the dotted curves are the monotonic stress–strain relationship of a bare bar. In the smeared stress–strain curves, stages 1T, 2T, 1C and 2C are the envelope curves and stages 3 and 4 are the unloading and reloading curves.

Envelope curves

For embedded steel bars, the envelope curves under cyclic loading closely resemble the monotonic stress–strain curves (Belarbi and Hsu 1994, 1995, and Hsu and Zhang 1996, Hoffman 2010). In Stages 1T and 2T, the relationship of the smeared stress (f_s) and smeared uniaxial strain ($\bar{\varepsilon}_s$) of an embedded steel bar can be described by equations for a bilinear model, as shown in Eqs. (28)-(30).

stage 1T $f_s=E_s\bar{\varepsilon}_s$ $(\bar{\varepsilon}_s\le\varepsilon_y')$ (28)

stage 2T $f_s=(1\text{-}0.096FF)(0.91\text{-}2B)f_y+(0.2FF+1)(0.02+0.25B)E_s\bar{\varepsilon}_s$ $(\bar{\varepsilon}_s>\varepsilon_y')$ (29)

$$B=1/\rho\left(f_{cr}/f_y\right)^{1.5} \tag{30}$$

where: E_s is the elastic modulus of rebar before yielding,

ε_y' is the yield strain of rebar, taken as $\varepsilon_y(0.93-2B)$, where ε_y is the yield strain of bare bar,

ρ is the steel ratio, and f_y is the yield stress of bare bar,

FF is the fiber factor in PSFC, for RC and PC *FF* is zero.

The smeared (average) constitutive relationships of embedded mild steel in compression are given as in Eqs. (31) and (32).

$$\text{Stage 1C} \qquad f_s = E_s\bar{\varepsilon}_s \qquad \bar{\varepsilon}_s \geq -\varepsilon_y' \qquad (31)$$

$$\text{Stage 2C} \qquad f_s = -f_y \qquad \bar{\varepsilon}_s < -\varepsilon_y' \qquad (32)$$

Unloading and reloading

The unloading and reloading stress vs. strain curves of embedded steel bars, stages 3 and 4, take into account the Bauschinger effect. This curve was found by Mansour *et al*. (2001) to be well represented by the Ramberg–Osgood type of expression first used by Yokoo and Nakamura (1977), as shown in Eq. (33).

$$\text{stage 3 and 4} \quad \bar{\varepsilon}_s - \bar{\varepsilon}_{si} = \frac{f_s - f_i}{E_s}\left[1 + A^{-R}\left|\frac{f_s - f_i}{f_y}\right|^{R-1}\right] \qquad (33)$$

where: f_i and $\bar{\varepsilon}_{si}$ are the smeared stress and smeared uniaxial strain of steel bars at the initial load reversal point,

the coefficients A and R taken as $1.9(\bar{\varepsilon}_p / \varepsilon_y')^{-0.1}$ and $10(\bar{\varepsilon}_p / \varepsilon_y')^{-0.2}$ to best fit the test data, where $\bar{\varepsilon}_p$ is the smeared uniaxial plastic strain of rebars.

2.5.4 Uniaxial constitutive relationship of prestressing steel

The smeared (average) stress(f_{ps}) and strain ($\bar{\varepsilon}_s$) relationships of prestressing tendons embedded in concrete (Wang 2006, Hoffman 2010) are given in Eqs. (34) and (35)

$$f_{ps} = E_{ps}\bar{\varepsilon}_s \qquad \bar{\varepsilon}_s < \frac{0.7f_{pu}}{E_{ps}} \qquad (34)$$

$$f_{ps} = \frac{E_{ps}''\bar{\varepsilon}_s}{\left[1+\left(\frac{E_{ps}''\bar{\varepsilon}_s}{f_{pu}'}\right)^m\right]^{\frac{1}{m}}} \qquad \bar{\varepsilon}_s \geq \frac{0.7f_{pu}}{E_{ps}} \qquad (35)$$

where: E_{ps} = elastic modulus of prestressing tendons taken as 200 GPa,

f_{pu} = ultimate strength of prestressing tendons taken as 1862 MPa,

E_{ps}'' = modulus of prestressing tendons in plastic region, taken as 209 GPa,

f_{pu}' = revised strength of prestressing tendons, taken as 1793 MPa,

m = shape parameter, taken as 4 for prestressing steel in PC and 5 for prestressing steel PSFC.

In the above equations, ℓp replaces ps in the subscript of symbols for the longitudinal

tendons, and tp replaces ps for the transverse tendons.

The cyclic behavior of mild steel can be extended to prestressing tendons. Hence during unloading and reloading stages, the stress strain relationship of prestressing tendons is the same as that of mild steel, as given by Eq. (33).

3. Finite element implementation

The constitutive laws discussed before are combined with the equilibrium and compatibility equations to form a tangent stiffness matrix $[D]$ for element.The details of the derivation of $[D]$ is presented in Zhong (2005). $[D]$is formulated as:

$$[D] = d\begin{Bmatrix}\sigma_x \\ \sigma_y \\ \tau_{xy}\end{Bmatrix} / d\begin{Bmatrix}\varepsilon_x \\ \varepsilon_y \\ \gamma_{xy}/2\end{Bmatrix} \tag{36}$$

$[D]$is evaluated by

$$[D] = \left[T(-\theta_1)\right][D_c][V]\left[T(\theta_1)\right] + \sum_i \left[T(-\theta_{si})\right][D_{si}]\left[T(\theta_{si}-\theta_1)\right][V]\left[T(\theta_1)\right] \tag{37}$$

In Eq. (37), $[D_c]$ is the uniaxial tangent constitutive matrix of concrete, $[D_{si}]$ is the uniaxial tangent constitutive matrix of steel, and $[V]$ is the matrix defined previously in Eq. (5). $[T(\theta_1)]$, $[T(-\theta_1)]$, $[T(\theta_{si}-\theta_1)]$ and $[T(-\theta_{si})]$ are the transformation matrixes.

The uniaxial constitutive matrix of concrete $[D_c]$is given by

$$[D_c] = \begin{bmatrix} \bar{\bar{E}}_1^c & \partial\sigma_1^c/\partial\bar{\varepsilon}_2 & 0 \\ \partial\sigma_2^c/\partial\bar{\varepsilon}_1 & \bar{\bar{E}}_2^c & 0 \\ 0 & 0 & G_{12}^c \end{bmatrix} \tag{38}$$

In Eq. (38), $\bar{\bar{E}}_1^c$ and $\bar{\bar{E}}_2^c$are the uniaxial tangent moduli of concrete in the 1 and 2directions, respectively, evaluated at a certain stress/strain state. The off-diagonal terms$\partial\sigma_1^c/\partial\bar{\varepsilon}_2$ and $\partial\sigma_2^c/\partial\bar{\varepsilon}_1$are obtained by using the uniaxial constitutive relationships and taking into account the states of the concrete stresses and uniaxial strains in the 1–2 directions, which are not zero because the stress and strain of the concrete in compression is softened by the orthogonal tensile strains.G_{12}^c is the shear modulus of concrete as described previously in Eq. (21).

The uniaxial stiffness matrix of rebars $[D_{si}]$ is evaluated as follows:

$$[D_{si}] = \begin{bmatrix} \rho_{si}\cdot\bar{\bar{E}}_{si} & 0 & 0 \\ 0 & 0 & 0 \\ 0 & 0 & 0 \end{bmatrix} \tag{39}$$

where $\rho_{si}$is the steel ratio in ith direction, and $\bar{\bar{E}}_{si}$ is the uniaxial tangent modulus for the rebars, as determined for a particular stress/strain state.

Adopting the OpenSees as framework, the finite element program named SCS developed for RC (Mo *et al*. 2008) was extended to include PC and PSFC by implementing the new constitutive modelsin OpenSees. Additional details about the finite element implementation can be obtained from Zhong (2005). This program is able to perform nonlinear finite element analysis of concrete structures under static, reversed cyclic, or dynamic loading.

4. Validation

The validation studies have been conducted by comparing the analytical results with tested results of seven series of tests. Some details about the experiments and simulations can be found in the Unified Theory of Concrete Structures by Hsu and Mo (2010).

4.1 Simulation of prestressed steel fiber concrete beams

Since PSFC beams were tested under monotonic loads, this validation and applicability of SCS program is only suitable in predicting the behavior of PSFC structures under monotonic loading. Finite element meshes of PSFC I-beams are shown in Fig. 5(a) and Fig. 5(b) for web-shear and flexural-shear respectively. The detailed description of the test specimens is referred to (Tadepalli 2011).

The measured and calculated load-displacement curves for PSFC beam tested in web-shear failure mode are shown in Fig. 6(a). It can be seen that the analysis predicts reasonably well the load-displacement characteristics of the beam including initial stiffness, post-cracking stiffness, yield displacement, and ultimate strength. The numerical simulation of this specimen was ended with the uniaxial strain in concrete reaching the ultimate value of 0.002.

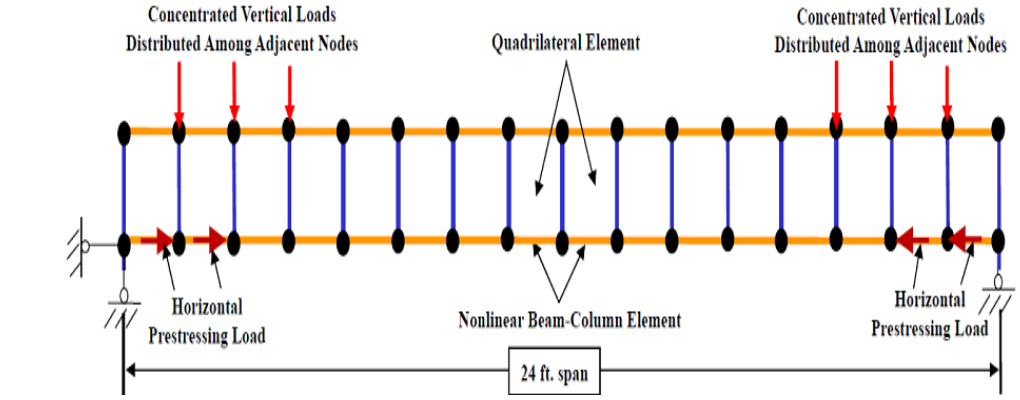

(a) tested under web-shear

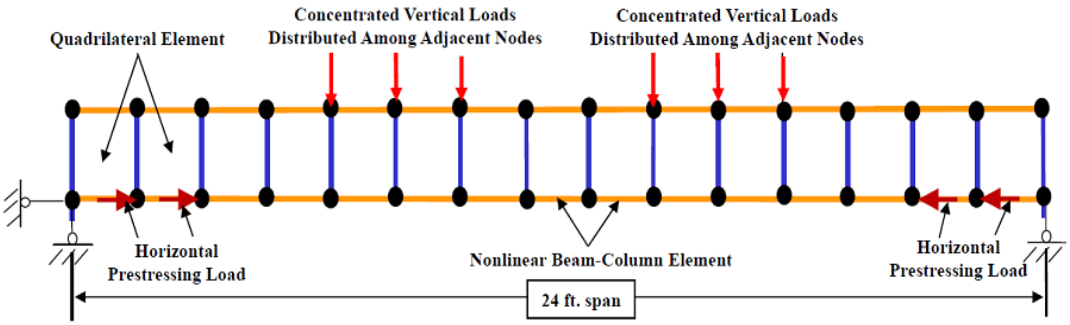

(b) tested under flexural-shear

Fig. 2 Finite element model of PSFC I-beams under web-shear

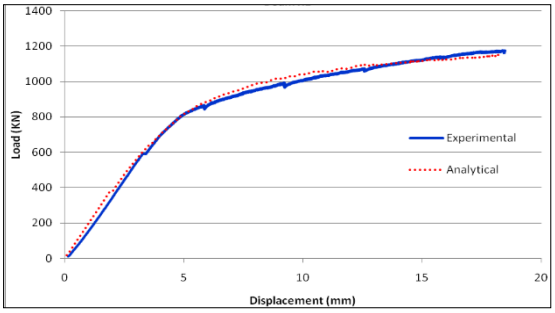

(a) under web-shear

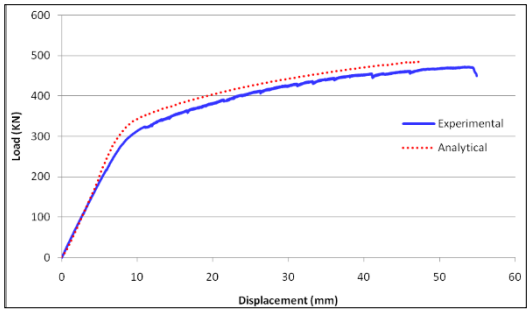

(b) under flexural-shear

Fig. 3 Comparison of experimental and analytical results of beam

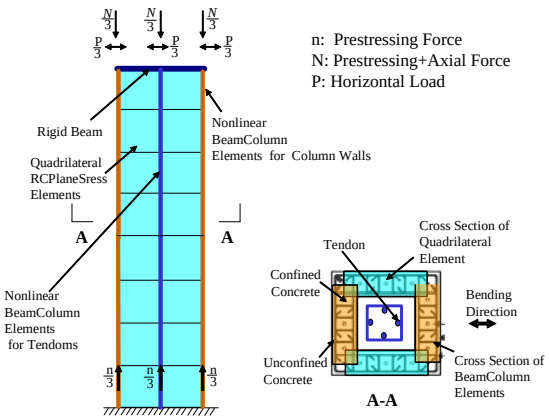

Fig. 4 Finite element model of post-tensioned columns

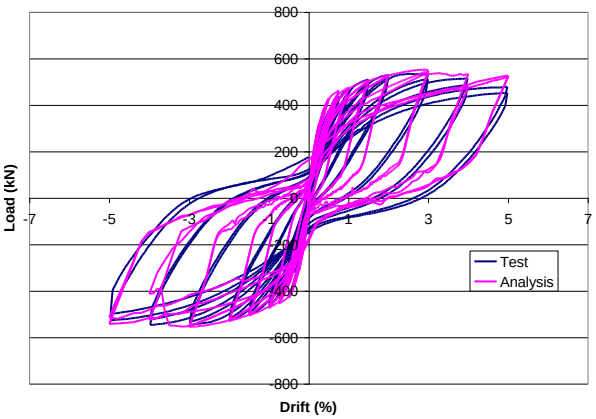

Fig. 5 Experimental and analytical load drift diagram of column specimen

The measured and calculated load-deformation curves for PSFC beam with flexure-shear failure are shown in Fig. 6(b). Compared with the experimental results, the analysis as well predicts the load versus deformation characteristics of the specimen including initial stiffness, post-cracking stiffness, yield displacement, and ultimate strength. The numerical simulation of this specimen was ended the uniaxial strain in the stirrups reaching the ultimate value and the load carrying capacity of the stirrups begin to decrease thereafter. Comparison of other aspects of test and analysis results including strain profiles along the cross-sections have also shown good agreement (Tadepalli 2011).

4.2 Post tensioned precast column under reversed cyclic loading

A full-scale post tensioned precast hollow bridge column has been tested at the State University of New York, Buffalo (Ou 2007). The column has a dimension of 860 mm × 860 mm with 200 mm thick walls. The height of the column is 4050 mm. The specimens were modeled by the finite element model shown in Fig. 7.

The analytical results of the load-drift relationships of the column specimen are illustrated by the pink hysteretic loops in Fig. 8. These pink loops are compared to the blue loops, representing

the experimental results. It can be seen that good agreements were obtained for the primary backbone curves, the initial stiffness, the yield point, the ultimate strength, and the failure state in the descending branch. The hysteretic behavior provided accurate measurements of the residual displacements, the ductility and the energy dissipation capacity of the specimen. Comparison of other aspects of test and analysis results including strain profiles along the cross-sections have also shown good agreement (Laskar 2009). The above-mentioned results verify the capability of SCS to predict the reversed cyclic behavior of prestressed concrete structures.

4.3 UH low-rse framed shear walls under reversed cyclic load

Nine 1/3-scale framed shear walls (Fig. 9), subjected to a constant axial load at the top of each column and a reversed cyclic load at the top beam, were performed at the University of Houston (Gao 1999). Finite element analyses of the nine specimens were conducted with model illustrated in Fig. 10.

The analytical and experimental results of the shear force-drift relationships of two shear walls

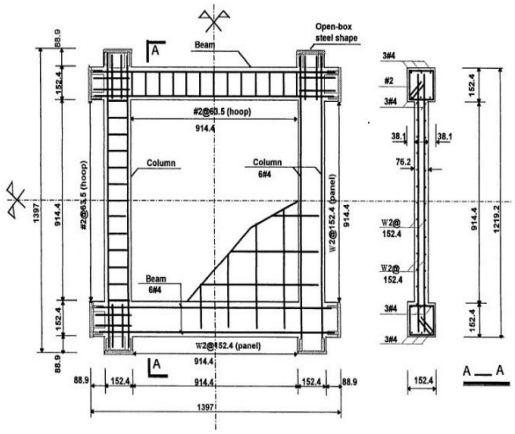

Fig. 6 Dimensions and steel arrangement of specimens

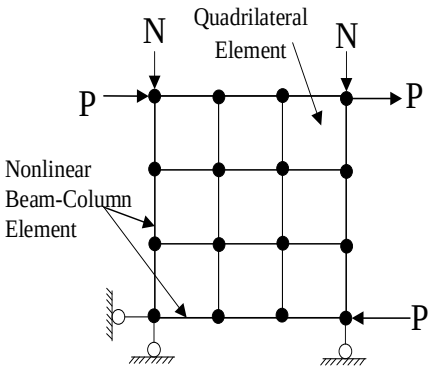

Fig. 7 Finite element modeling of the wall

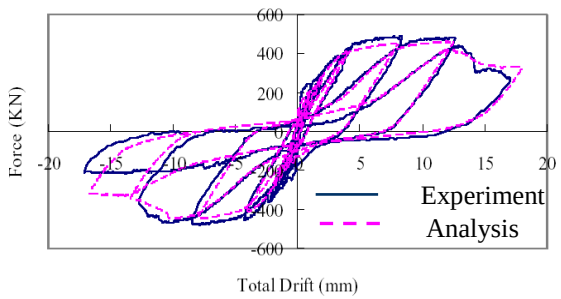

(a) FSW13 (P/P_0=0.07, ρ_w=0.23%)

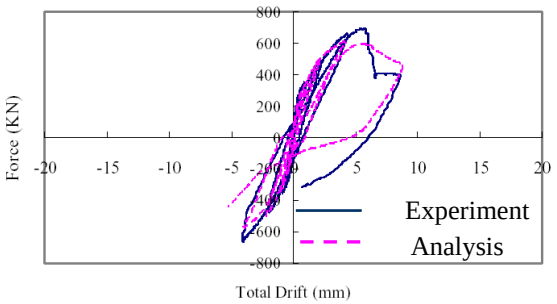

(b) FSW12 (P/P_0=0.4, ρ_w=0.23%)

Fig. 8 Shear force - Drift Displacement of Specimens FSW13 and FSW12 (P/P0 is the magnitude of vertical load on each column,ρ_w is the steel ratio in the shear wall)

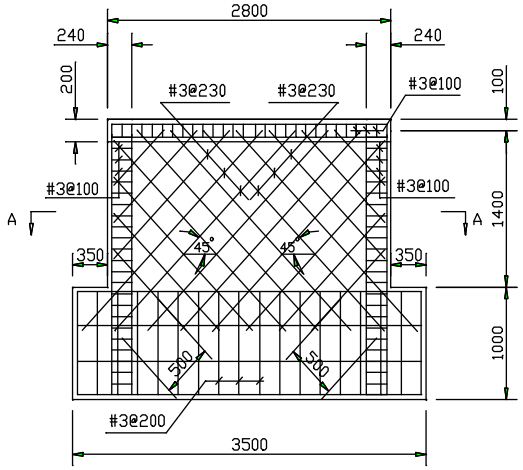

Fig. 9 Dimensions and reinforcement of specimen RLB

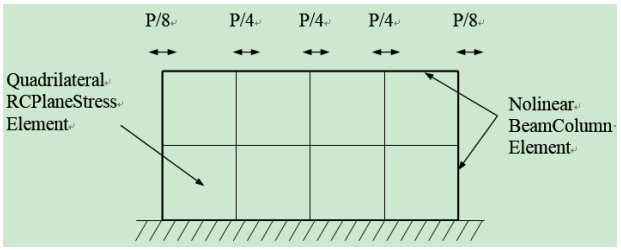

Fig. 10 Finite element mesh of specimens RLB

are illustrated in Fig. 11. It can be seen that good agreements were obtained for the primary backbone curves, including the initial stiffness, the yield point, the ultimate strength, and the failure state in the descending branch. The hysteretic behavior provides accurate measurements of the pinching effect, the residual displacements, the ductility and the energy dissipation capacity in all specimens. Even the failure modes can be predicted by the CSMM-based finite element program. Fig. 11 shows that SCS was capable of capturing the ductile and brittle failure behavior of specimens FSW13 and FSW12, respectively. In fact, the analytical and experimental results for the other seven specimens were also in good agreement (Zhong 2005). Detailed comparison of other aspects of test and analysis results including strain profiles along the cross-sections have also shown good agreement (Zhong 2005).

4.4 Low-rise framed shear wall under reversed cyclic load

A low-rise shear wall (RLB) was tested under reversed cyclic horizontal loading at National Center for Research on Earthquake Engineering, Taipei, Taiwan (NCREE). The specimen and its finite model are shown in Fig. 12 and Fig. 13. Reversed cyclic horizontal loads were applied on the top of the shear wall, and reversed cyclic analyses were conducted on the specimen (Zhong 2005).

The observed and calculated load-displacement relationships for specimen RLB are shown in Fig. 14. Compared with the experimental results, the analyses accurately predicted the load versus displacement characteristics including precracking stiffness, postcracking stiffness, ultimate strength, residual displacement, and energy dissipation. The envelopes including ascending and descending branches of the specimen, which show the typical type of shear failure, were accurately predicted by the analytical results. Detailed comparison of other aspects of test and analysis results including strain profiles along the cross-sections have also shown good agreement (Zhong 2005).

4.5 Mid-rise famed shear wall under reversed cyclic load

A mid-rise shear wall (RMB) was tested under reversed cyclic horizontal loading at NCREE. The dimensions and reinforcements of the specimen are shown in Fig. 15, and finite element model of the specimen is shown in Fig. 16. Reversed cyclic horizontal loads were applied on the top of the shear wall (Zhong 2005).

The experimental and calculated load-displacement relationships for the specimen are shown in Fig. 17. Compared with the experimental results, the analyses accurately predicted the load versus displacement characteristics including precracking stiffness, postcracking stiffness, ultimate strength, residual displacement, and energy dissipation. The nearly flattop envelopes of the specimen, which is a typical behavior of the flexure mechanism, were also predicted by the analyses. Detailed comparison of other aspects of test and analysis results including strain profiles along the cross-sections have also shown good agreement (Zhong 2005). Analysis results of specimens discussed in Sections 4.4 and 4.5 demonstrates the capability of SCS to predict the cyclic behavior of various types of shear critical structures such as shear walls.

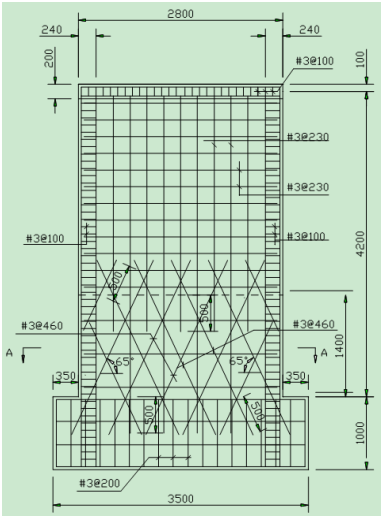

Fig. 11 Dimensions and reinforcement of specimen RMB

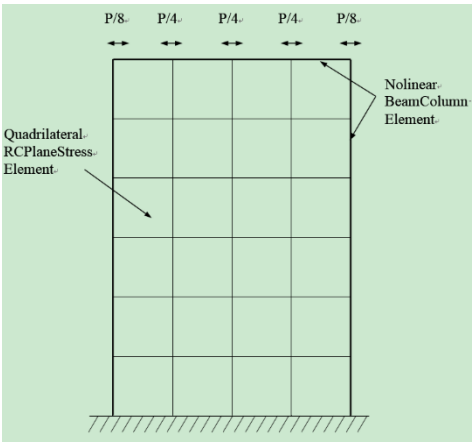

Fig. 12 Finite element mesh of specimens RMB

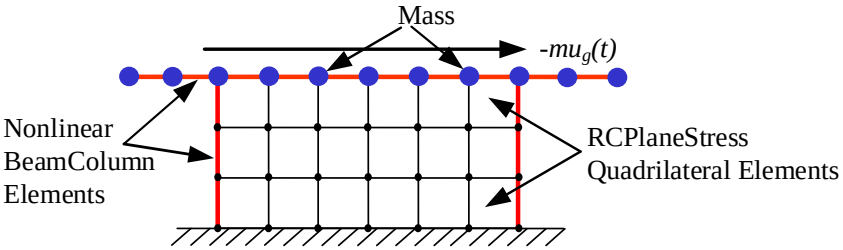

Fig. 13 Wall elevation in finite element mesh

4.6 Framed shear walls under shake table excitations

Two low-rise shear walls with a height-to-width ratio of 0.5 were tested on a shake table under seismic excitations at NCREE (Zhong 2005). The two specimens were designed identically with the exception of the steel grid orientation in the walls. While one specimen (STC) was designed as a conventional shear wall with the steel grid in the horizontal and vertical directions (Fig. 18(a)), the reinforcement in the other specimen (STN) was oriented at 45 degrees to the horizontal (Fig. 18(b)). Accelerometers were placed on the shake table and the top slab to measure the actual acceleration of the shake table and the response acceleration of the specimen. Finite element model used for analysis is illustrated in Fig. 19.

The analysis for the first two runs was omitted because the response of the specimen was too small when compared with the remaining test runs. Damping proportional to the converged stiffness at each time step was applied to model the energy dissipation arising from story deformations. The damping ratios were determined based on the different damage levels of the specimens (Hsu and Mo 2010).

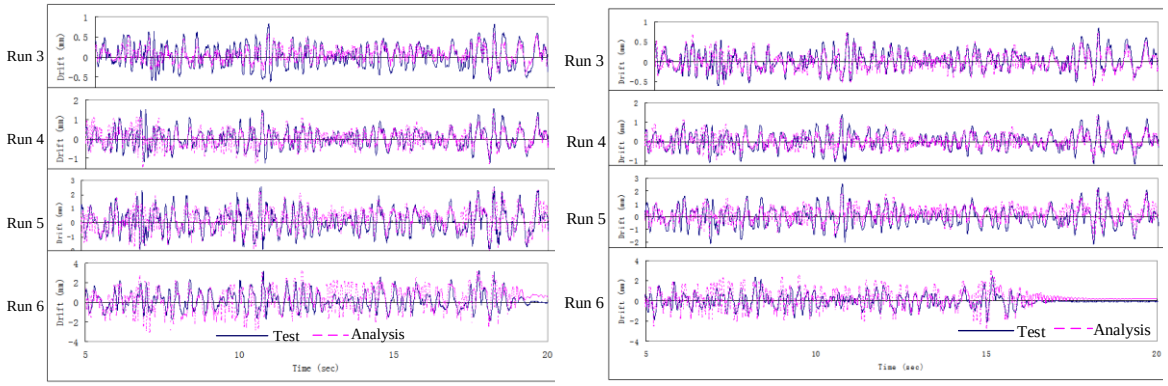

(a) STC (b) STN

Fig. 14 Measured and computed drift time history of specimen STC and STN

Fig. 15 A seven-story wall building tested at UCSD

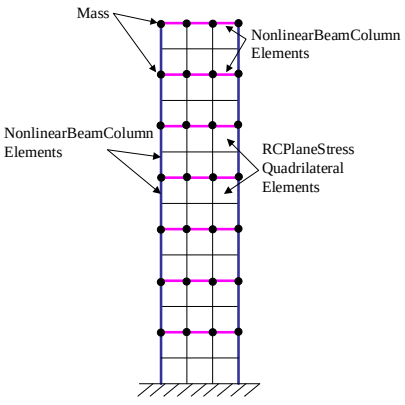

Fig. 16 Finite element model

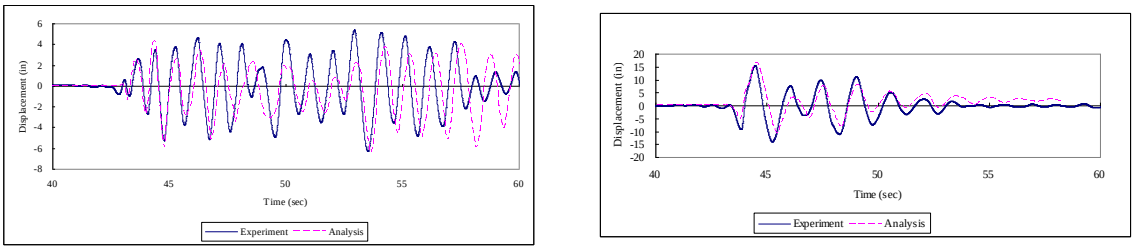

(a) EQ3 Run (b) EQ4 Run

Fig. 17 Time histories of measured and calculated displacement at building top

The calculated drift and time history of specimens STC and STN for the third to the sixth runs are presented in Fig. 20 (a) and (b), respectively. The computed drift and time histories show good agreement with the measured responses for both specimens. In the sixth run, the analyses slightly overestimated the drifts for both specimens. The results also show that the damping ratios used in the analyses were appropriate to take into account the different damage levels of the structures. Detailed comparison of other aspects of test and analysis results including strain profiles along the cross-sections have also shown good agreement (Zhong 2005). The above mentioned results demonstrate the efficiency of SCS in predicting the actual seismic behavior of shear critical concrete structural components.

4.7 A seven-story wall building under shake table excitations

A full-scale seven-story reinforced concrete wall building (Fig. 21) was tested on the shake table located at UCSD's Engelkirk Structural Engineering Center (Zhong 2005). The building was composed of a web wall, a flange wall, a post-tensioned precast pier, gravity columns, and slabs at each floor. The building was subjected to four increasing intensity of uniaxial earthquake ground motions (EQ1, EQ2, EQ3 and EQ4). It is assumed that the flange wall, precast pier and foundation of the seven-story building do not transfer shear loads acting on the structure and hence these components of the building have been neglected and the building was simplified to a 2-D finite element model, as shown in Fig. 22.

For simplicity, time histories of the predicted displacement at the top of the building and measured test data for EQ3 and EQ4 are presented in Fig. 23. It can be seen from Fig. 23 that the prediction of the displacement is close to the measured results both in the vibration frequency and displacement magnitude. The above-mentioned results demonstrate the capability of SCS to predict the behavior of large full-scale shear critical concrete structures under seismic loading.

5. Conclusions

The constitutive models of CSMM for reinforced, prestressed and prestressed steel fiber concrete elements subjected to seismic shear were determined by testing full scale reinforced and prestressed as well as prestressed steel fiber concrete panels using the Universal Panel Tester available at the University of Houston. Adopting the OpenSees as the finite element development framework, the finite element program named SCS developed for RC previously was extended to include PC and PSFC by implementing the constitutive models in OpenSees. The developed finite

element program was validated by tests on prestressed steel fiber concrete beams under monotonic loading, post tensioned precast concrete column under reversed cyclic loading, framed shear walls under reversed cyclic loading or shaking table excitations, and a seven-story wall building under shake table excitations. Non-linear beam column elements (previously incorporated in OpenSees by other researchers) were used to model structural components carrying flexural loads. Since the constitutive models are proposed for shear critical structures, they have not been used to create the non-linear beam column elements. The comparison of analytical results with test outcomes indicates good agreement. All the numerical simulations of the test specimens were ended with the uniaxial strains in the materials reaching their ultimate values. The model have not been used to predict the cyclic/seismic behavior of PSFC since no suitable test results for PSFC shear-critical structures under reversed cyclic loading has been found in literature. However since the model can well predict the monotonic behavior of PSFC, the reversed cyclic behavior of PC and the reversed cyclic as well as seismic behavior of RC, it is expected to also accurately predict the reversed cyclic and seismic behavior of PSFC when such test data becomes available.

Acknowledgments

The authors would like to express their gratitude to the following sponsors for this project. They are the China Government Scholarship Program, Kwan Hua Scholarship Foundation, and Research Institute of Structural Engineering and Disaster Reduction (Proj. No. SLDRCE-MB-01), Tongji University, China. The materials presented are the research findings by the authors, and are not necessarily expressed for the funding agencies' opinion.

References

Belarbi, A. and Hsu, T.T. (1994), "Constitutive laws of concrete in tension and reinforcing bars stiffened by concrete", *ACI Struct. J.*, **91**(4), 465-474.

Belarbi, A. and Hsu, T.T. (1995), "Constitutive laws of softened concrete in biaxial tension compression." *ACI Struct. J.*, **92**(5), 562-573.

Gao, X.D. (1999), "Framed shear walls under cyclic loading", Ph.D. Dissertation, University of Houston, Houston.

Hoffman, N.S. (2010), "Constitutive relationships of prestressed steel fiber concrete membrane elements", Ph. D. Dissertation, University of Houston, Houston.

Hsu, T.T. and Mansour, M.Y. (2005), "Stiffness, ductility, and energy dissipation of rc elements under cyclic shear", *Earthq. spectra*, **21**(4), 1093-1112.

Hsu, T.T. and Mo, Y.L. (2010), Unified Theory of Concrete Structures, Wiley, Chichester, West Sussex, U.K.

Hsu, T.T. and Zhang, L.X. (1996), "Tension stiffening in reinforced concrete membrane elements", *ACI Struct. J.*, **93**(1), 108-115.

Hsu, T.T. and Zhu, R.R. (2002), "Softened membrane model for reinforced concrete elements in shear", *ACI Struct. J.*, **99**(4), 460-469.

Hsu, T.T.C. (1993), Unified theory of reinforced concrete, CRC Press, Boca Raton, FL.

Lu, X., Urukap, T.H., Li, S. and Lin, F. (2012), "Seismic behavior of interior RC beam-column joints with additional bars under cyclic loading", *Earthq. Struct.*, **3**(1), 37-57.

Mansour, M. and Hsu, T.T. (2005a), "Behavior of reinforced concrete elements under cyclic shear. I: experiments", *J. Struct. Eng.*, **131**(1), 44-53.

Mansour, M. and Hsu, T.T. (2005b), "Behavior of reinforced concrete elements under cyclic shear. II: Theoretical model", *J. Struct. Eng.*, **131**(1), 54-65.
Mansour, M., Lee, J.Y. and Hsu, T.T. (2001), "Cyclic stress-strain curves of concrete and steel bars in membrane elements", *J. Struct. Eng.*, **127**(12), 1402-1411.
Mansour, M.Y. (2001), "Behavior of reinforced concrete membrane elements under cyclic shear: experiments to theory", Ph. D. Dissertation, University of Houston, Houston.
Mo, Y.L., Zhong, J. and Hsu, T.T. (2008), "Seismic simulation of RC wall-type structures", *Eng. Struct.*, **30**(11), 3167-3175.
Moretti, M.L. and Tassios, T.P. (2013), "Design in shear of reinforced concrete short columns", *Earthq. Struct.*, **4**(3), 265-283.
OpenSees (2013), "Open system for earthquake engineering simulation", http://opensees.berkeley.edu/.
Ou, Y.C. (2007), "Precast segmental post-tensioned concrete bridge columns for seismic regions", Ph.D. Dissertation, State University of New York, Buffalo.
Pang, X.B. and Hsu, T.T. (1995), "Behavior of reinforced concrete membrane elements in shear", *ACI Struct. J.*, **92**(6), 665-679.
Pang, X.B. and Hsu, T.T. (1996), "Fixed angle softened truss model for reinforced concrete", *ACI Struct. J.*, **93**(2), 197-207.
Tadepalli, P.R. (2011), "Shear behavior of prestressed steel fiber concrete girders", Ph.D. Dissertation, University of Houston.
Vecchio, F.J. and Collins, M.P. (1981), *Stress-Strain Characteristics of Reinforced Concrete in Pure Shear*, IABSE Colloquium, Advanced Mechanics of Reinforced Concrete, Delft, Final Report, Zurich, Switzerland.
Vecchio, F.J. and Collins, M.P. (1986), "The modified compression-field theory for reinforced concrete elements subjected to shear", *ACI J.*, **83**(2), 219-231.
Wang, J. (2006), "Constitutive relationships of prestressed concrete membrane elements", Ph.D. Dissertation, University of Houston, Houston.
Xing, G., Wu, T., Niu, D. and Liu, X. (2013), "Seismic behavior of reinforced concrete interior beam-column joints with beams of different depths", *Earthq. Struct.*, **4**(4), 429-449.
Yokoo, Y. and Nakamura, T. (1977), "Nonstationary Hysteretic Uniaxial Stress–Strain Relations of a Steel Bar", *Transact. Architect. Inst. Japan*, (260), 71-80.
Zhong, J. (2005), "Model-based simulation of reinforced concrete plane stress structures", Ph.D. Dissertation, University of Houston, Houston.
Zhu, R.R. and Hsu, T.T. (2002), "Poisson effect in reinforced concrete membrane elements", *ACI Struct. J.*, **99**(5), 631-640.
Zhu, R.R., Hsu, T.T. and Lee, J.Y. (2001), "Rational shear modulus for smeared-crack analysis of reinforced concrete", *ACI Struct. J.*, **98**(4), 443-450.